Diffusion of O atoms on a CO-covered Ru(0001) surface – a high-speed STM and DFT study at an enhanced CO coverage

Hannah Illner[1], Sung Sakong[2], Ann-Kathrin Henß[1], Axel Groß[2], Joost Wintterlin[1,3]*

[1]Department of Chemistry, Ludwig-Maximilians-Universität München, 81377 Munich, Germany

[2]Institute of Theoretical Chemistry, University of Ulm, 89081 Ulm, Germany

[3]Center for NanoScience, Schellingstr. 4, 80799 Munich, Germany

*Corresponding author

Abstract

The diffusion of adsorbed O atoms on a CO-covered Ru(0001) surface has recently been explained by a "door-opening" mechanism which is driven by fluctuations in the CO layer. Here we analyze how this mechanism changes at a higher CO coverage and therefore lower concentrations of empty sites. High-speed scanning tunneling microscopy was used to track the motions of the O atoms. A statistical model based on nearest-neighbor jumps and uniform hopping probabilities into the six equivalent directions of the Ru(0001) lattice describes the data well. Surprisingly, the extracted hopping rates, which involve site exchanges with CO molecules, are faster than the site exchanges at the lower coverage. Density functional theory calculations were performed to explain these observations. The configurations of the CO molecules around the adsorbed O atoms obtained at the higher CO coverage are disordered. Displacements of CO molecules cost less energy than displacements in the ordered $(\sqrt{3} \times \sqrt{3})R30°$ structure of the previous study. In addition, the activation energies for the jumps of the O atoms are lowered by enhanced O/CO repulsions. The atomic processes are thus faster at the higher coverage, but the general features of the door-opening mechanism remain valid.

1

Introduction

Surface diffusion of adsorbed particles is an essential step in heterogeneous catalysis. It determines the frequency at which the reacting particles on a catalyst surface collide with each other and the speed at which they can move to an active site. Less obviously, assumptions about the speed of surface diffusion also underlie microkinetic models of catalytic reactions. Microkinetic models are based on rate equations which contain the coverages Θ_i of the adsorbed species i as variables.[1-3] By using coverages it is implicitly assumed that the occupation probability of a given adsorption site is identical to the global coverage. A necessary condition that this assumption is fulfilled is that surface diffusion, which mixes the adsorption layer, is fast. More precisely, it has to be faster than the other steps of a catalytic reaction, i.e., all the adsorption, reaction, and desorption steps, which permanently disturb the statistical occupation of the adsorption sites.

The assumption of fast surface diffusion is probably always fulfilled when adsorbate coverages are low. In these cases the fact applies that the hopping barrier seen by an adsorbed particle, i.e., the activation energy to jump from one adsorption site to the next, is low, at least for the typical metals used as catalysts.[4] However, at the high pressures of industrial catalytic processes, coverages of coadsorbed reactant species and intermediates may be appreciable. Under these conditions, the speed of surface diffusion may not be determined by a hopping barrier but by the availability of empty sites. Macroscopic diffusion coefficients in fact suggest that, as coverages of coadsorbates increase, the surface mobility of a tracer particle can decrease strongly.[5-10]

However, in a recent study we have observed a new 2D lattice diffusion mechanism that can keep surface mobility of an adsorbed particle high in a relatively dense coadsorption layer.[11, 12] On a Ru(0001) surface, individual O atoms adsorbed in a layer of coadsorbed CO molecules travel through the CO matrix by, as we termed it, a door-opening mechanism. According to this mechanism, the O atoms, which are adsorbed in vacancies of the CO layer, are intermediately trapped in cages formed by the neighboring CO molecules. However, there are rapid density fluctuations in the CO layer, and when such a fluctuation happens near the position of an O atom, a "door is opened", through which the O atom can leave its cage on a low-energy path. The mechanism is different from the standard vacancy mechanism known for diffusion in 3D lattices[13] and also observed for 2D systems of metal surfaces with alloyed-in atoms of a foreign metal.[14-16] In the standard vacancy mechanism, a tracer atom can only jump to a new site when a mobile vacancy of the host lattice comes close to the tracer atom. By contrast, in the door-opening mechanism, fluctuations happen permanently at all locations, and the statistics and the directions of the hopping events are different. The mechanism is also different from other diffusion mechanisms observed on adsorbate-covered solid surfaces.[17, 18] In the mentioned case of O atoms in a CO matrix on a Ru(0001) surface, the resulting mobility of the O atoms was almost as high as on the bare Ru surface.[11, 12]

Here we present a study by high-speed scanning tunneling microscopy (STM) in which we have investigated how the door-opening mechanism changes when the CO coverage is increased. In the previous study the CO molecules formed a $(\sqrt{3}\, x\, \sqrt{3})R30°$ structure with a CO coverage of

2

0.33 monolayers (ML).[11, 12] Hence, 2/3 of the CO adsorption sites were not occupied. Empty sites are required both for the fluctuations of the CO layer and for the jumps of the O atoms. By increasing the CO coverage to higher values than 0.33 we had expected that the mobility of the O atoms would decrease because more sites are blocked by CO molecules. Surprisingly, we find the opposite, the diffusion is faster than at Θ_{CO} = 0.33 ML. It is even faster than on the bare Ru(0001) surface without any coadsorbed CO. To understand these observations, the energetics of the diffusion process was evaluated by density functional theory (DFT). The individual atomic steps extracted from this analysis are different in detail from those at Θ_{CO} = 0.33 ML, but the general physical effect that fluctuations enable diffusion is in line with the door-opening mechanism. That the mechanism remains valid also in this more complex situation suggests that it may play a general role in catalytic reactions.

Experimental

The experiments were performed in an ultra-high vacuum (UHV) chamber at a base pressure below 1 x 10^{-10} mbar. In addition to the STM, the system is equipped with facilities for Auger electron spectroscopy (AES) and low-energy electron diffraction (LEED). The home-built beetle-type STM has specially been designed for studies of the dynamics of surface processes. It combines temperature variability with video-rate imaging. A sample mounted to the STM can simultaneously be cooled by liquid He and radiatively heated by a filament; temperatures between 50 and 500 K can be adjusted in this way. At the same time, the STM can be operated in a fast mode in which it produces movies at frame rates of typically 10 frames s^{-1}. Frame rates of up to 50 frames s^{-1} have also been realized. Scanning the tip in the constant-height mode together with several modifications of the setup, in particular of the STM electronics and of the data acquisition system, allow for this video-rate imaging. Technical details have been published previously.[19]

The Ru(0001) sample was prepared by Ar ion sputtering [1 kV, p(Ar) = 6.4 x 10^{-5} mbar, ion current at the sample 4.2 µA, 10 – 15 min] and oxidation of carbon, the main contaminant. For oxidizing higher amounts of carbon, oxygen pressures of 2.7 x 10^{-7} mbar were applied for 10 – 15 min at 910 K, while for lower carbon coverages 2 – 20 L of O_2 were dosed at 298 - 423 K. [Dosages are given in Langmuirs (L), with 1 L = 1.33 x 10^{-6} mbar s.] Then the sample was flash-annealed to 1700 K to desorb remaining oxygen. This preparation sequence was repeated until the sample was clean in AES. Shortly before starting the STM experiments, the sample was again flash-annealed to 623 K to remove CO that may have readsorbed from the residual gas during cooling down after the high-temperature flash.

A difficulty with the preparation of Ru samples is the overlap in AES of the main KLL peak of carbon at ~272 eV with the MNN peak of ruthenium at 273 eV. Residual carbon was therefore determined indirectly. The KLL peak of graphitic carbon is strongly asymmetric whereas the Ru_{MNN} peak is almost symmetric, so that the asymmetry of the overall peak can serve as a measure of the (graphitic) carbon coverage.[20-22] Other forms of carbon cannot be detected by this method, but in the STM, after prolonged sample preparation, no identifiable contaminants were observed, except for low coverages

of N atoms (Θ_N = 0.002 ML), the origin of which could not be clarified. To prepare the layers of CO molecules with embedded O atoms, O_2 and CO were adsorbed by backfilling the chamber.

To extract the trajectories of the diffusing O atoms from the STM movies special software was applied that can identify, localize, and track mobile adsorbed particles. It makes use of a wavelet-based algorithm and has been described in a recent publication.[23]

Calculational method

The potential energy surface (PES) of the adsorbed O atoms and CO molecules on the Ru(0001) surface was determined by periodic density functional theory (DFT) calculations using the VASP software package.[24] Exchange-correlation effects were evaluated using a revised version of the Perdew-Burke-Ernzerhof (RPBE) functional[25], and the ionic cores were described by the projector augmented wave (PAW) potential.[26] The electronic wave functions of quasi-one-particle states were expanded up to 350 eV using a plane-wave basis set. Van der Waals interactions between the adsorbed particles and between the adsorbates and the first layer of the Ru slab were included by employing the semiempirical D3 dispersion correction scheme, as suggested by Grimme.[27, 28] By combing RPBE functional and D3 corrections, adsorbate/metal surface interactions can be evaluated accurately.[29-31]

The Ru(0001) surface was modeled by a slab consisting of three atomic layers with optimized bulk Ru lattice parameters a = 2.74 Å and c = 1.58. The topmost Ru layer of the slab and the adsorbates were fully relaxed to optimize local energy minimum configurations with a force convergence criterium of 0.01 eV/Å. The first Brillouin zone was integrated using a $3x3x1$ k-point mesh for the $(6 \, x \, 6)$ surface unit cell. The slabs were separated by 15 Å of vacuum, and a compensating dipole field was used to correct the surface dipole to avoid any spurious interactions between the periodic images.

The CO-covered surface was modeled by CO molecules at on-top sites, and the coverage was varied from 0.02 to 0.75 ML. Several ordered CO structures were considered, namely a $(3 \, x \, 3)$, a $(2 \, x \, 2)$, a $(\sqrt{3} \, x \, \sqrt{3})R30°$, and a $(2\sqrt{3} \, x \, 2\sqrt{3})R30°$ structure, and also many locally disordered CO structures. The CO molecules adsorb in an upright manner through the C atom when the neighboring Ru sites are free of CO molecules. When CO molecules are placed on adjacent Ru sites, the molecules tilt away from each other to reduce repulsive interactions. The disordered configurations were constructed by adding or removing CO molecules from ordered structures and/or by displacing CO molecules from sites in the ordered structures to neighboring sites. Altogether 105 different CO configurations were analyzed. The CO adsorption energies of the various structures (E_{ads}) are treated as relative values, i.e., with respect to the adsorption energy of an isolated CO molecule on the bare Ru(0001) surface:

$$E_{ads} = \frac{E_{tot} - E_{\text{Ru(0001)}} - n_{\text{CO}}E_{\text{CO}} - n_{\text{O}}E_{\text{O}}}{n_{\text{CO}}}$$

E_{tot} is the energy of the total system, $E_{\text{Ru(0001)}}$ is the energy of the uncovered Ru(0001) slab, E_{CO} and E_{O} are the adsorption energies of an isolated CO molecule and O atom, respectively, and n_{CO} and n_{O} are the numbers of the respective particles in the cell. DFT calculations tend to overestimate the

4

adsorption energy of CO by 0.3 eV with respect to the gas phase.[31-33] However, by referring to an isolated CO adsorbate, as is done here, this error can be neglected. In practice, by defining E_{ads} in this way, it becomes identical to the interactions between the particles. The activation barriers of the particle jumps are calculated by the nudged elastic band method[34] with four images.

Results and discussion

In the experiments it turned out that, in the temperature range where the moving O atoms could be tracked by the STM (239 to 280 K), the surrounding CO matrix could not be resolved, a result of the fast fluctuations of the CO layer. To nevertheless get information about the CO matrix, preparatory experiments at lower temperatures were performed. The O/CO layer was prepared by gas dosing when the crystal, which was still mounted to the sample manipulator, cooled down after the final flash annealing. When the temperature had decreased to approximately 370 K, 0.05 L of O_2 were dosed, and when the temperature had further fallen to approximately 345 K, 50 L of CO were dosed. Dosing at these still somewhat elevated temperatures made it easier preparing CO layers with defined coverages in a controlled way, whereas dosing at lower temperatures quickly led to CO phases with higher coverages than intended here. Moreover, the formation of metastable phases was avoided in this way. After dosing, the sample was transferred to the liquid He-cooled STM where the temperature further decreased to 70 K.

Figure 1(a) shows an STM image obtained after this procedure. It was recorded in the standard slow, constant current mode and shows a characteristic "leopard skin" pattern of partially open rings. The pattern mainly represents the layer of CO molecules that, at 70 K, is almost frozen, so that the structure could be resolved. The embedded O atoms are hard to see in these low temperature data – a few, very dark sites in figure 1(a) are likely positions – but the oxygen becomes apparent in the blurred CO layer at higher temperatures (see below).

Similar images have been obtained by Chen et al. in a low-temperature (4.5 K) STM investigation of pure CO phases on Ru(0001).[35] In this study, the authors could distinguish two states of the tunneling tip, a metallic one and one with a CO molecule at the apex of the tip. When the tip had an attached CO molecule, the adsorbed CO molecules on the Ru surface appeared as simple maxima (bright in the constant current data). When the tip was metallic, the contrast was more complex. The STM image of figure 1(a) is similar to the images taken with the metallic tip. When we follow the interpretation of the Chen study, a full, slightly hexagonally deformed bright ring [figure 1(b), red mark] represents a cluster of seven CO molecules adsorbed on neighboring $(1 \, x \, 1)$ sites [figure 1(c)]. The center CO molecule of the cluster appears dark and the outer six molecules appear bright, and the edges of the hexagon are rotated by 30° with respect to the positions of the outer six CO molecules. Similar images (of the pure CO layer) have also been reported by Lechner et al.[36] Previous work by electron stimulated desorption of ions angular directions (ESDIAD) and DFT showed that the outer CO molecules of the clusters are tilted by a few degrees away from the center CO molecule.[37, 38] This difference in bonding

geometry may explain the different imaging of the center and the outer CO molecules by the STM. Incomplete rings and smaller fractions of rings would accordingly represent clusters of only six or fewer CO molecules [figures 1(b) and (c)]. That all CO molecules in the structure occupy on-top sites is based on previous vibrational spectroscopy studies.[39, 40]
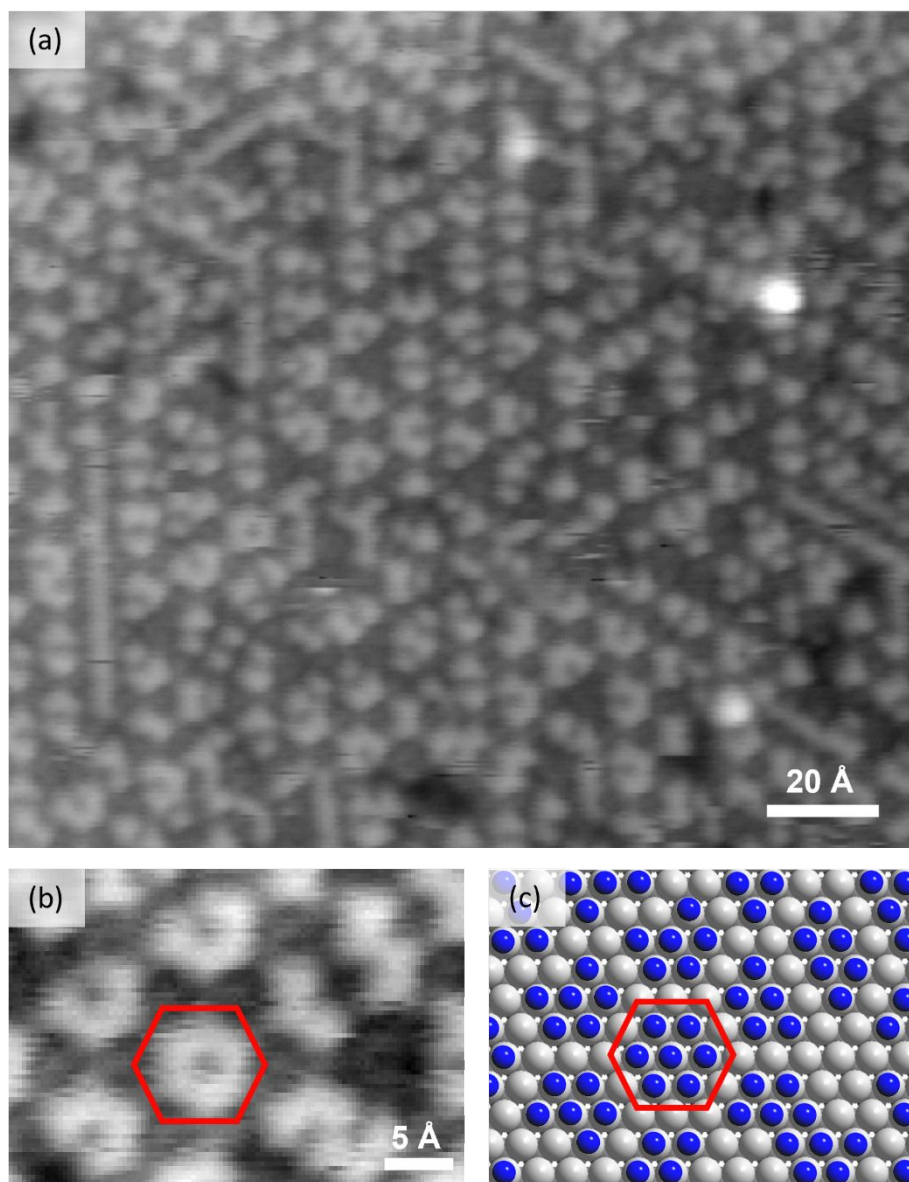
Figure 1: Partially disordered $(2\sqrt{3} \times 2\sqrt{3})R30°$ CO structure on the Ru(0001) surface. (a) Large-scale STM image of the surface with Θ_{CO} = 0.47 ML, recorded in the constant current mode (70 K, tunneling voltage V_t = -1.00 V, tunneling current I_t = 3 nA,). (b) Small-scale STM image under the same conditions as in (a); the red hexagon marks a cluster of seven CO molecules. (c) Structure model of the area shown in (b); CO molecules indicated in blue, Ru atoms in grey.

Figure 1(a) shows that the CO clusters are not randomly distributed but arranged in a hexagonal, partially ordered pattern. Its periodicity and orientation with respect to the metal surface it close to a $(2\sqrt{3} \times 2\sqrt{3})R30°$ structure, a well-known CO structure on Ru(0001) from LEED experiments.[41, 42] For the perfect $(2\sqrt{3} \times 2\sqrt{3})R30°$ structure a structure model has been proposed by McEwen and Eichler

6

and by Chen et al. that consists of complete clusters of seven CO molecules, arranged in the same manner as the incomplete clusters in figure 1(c).[35, 38] The CO coverage of the perfect $(2\sqrt{3} \: x \: 2\sqrt{3})R30°$ structure is 7/12 = 0.58 ML. For the present study, we can conclude that the described preparation leads to a CO layer that, when cooled to 70 K, displays an incomplete $(2\sqrt{3} \: x \: 2\sqrt{3})R30°$ structure. Like the perfect $(2\sqrt{3} \: x \: 2\sqrt{3})R30°$ structure it is formed by clusters of CO molecules, but the clusters contain fewer than seven molecules.

Figure 2 shows two STM frames from a movie of the same state of the surface as figure 1 (70 K), recorded in the fast mode. That the noise level is higher and the pixel resolution lower than in the standard slow, constant current mode is typical of the fast mode.[23] Nevertheless, one can recognize the same "leopard skin" pattern in figure 2(a) as in figure 1(a) (not the same surface area). The contrast is inverted, i.e., CO appears dark, a result of the constant height mode in which the contrast is inverted when the tunneling voltage V_t is switched from a positive to a negative value (the movie was recorded with a negative V_t).

Figure 2(b), which is from the same movie and surface region, was taken two images earlier than (a). Before this frame, the contrast was the same as in figure 2(a). Then, while recording the frame of figure 2(b), the tunneling tip suddenly changed (arrow mark), after which the contrast was different. This contrast change resembles the observations by Chen et al. when a CO molecule became attached to the tip;[35] the tip change resolved in figure 2(b) may indicate such an event. With the changed contrast, the ring fragments that appear empty in figure 2(a) display an additional dark dot in their centers, and the more or less continuous rings and ring fragments have separated into well-defined atomic features. Obviously, with this state of the tip the individual CO molecules are resolved. This allowed us to construct precise models of the CO configurations, and figure 2(c) shows the configuration in the marked regions of the STM images. The model confirms the above proposal that the CO molecules form hexagonal, partially ordered arrangements of clusters. As the clusters contain fewer than the ideal seven molecules, the CO coverage is lower than Θ_{CO} = 0.58 ML of the perfect $(2\sqrt{3} \: x \: 2\sqrt{3})R30°$ structure. The coverage is approximately 0.47 ML, and all oxygen diffusion measurements were performed with CO coadsorption layers of this coverage.

To test whether DFT reproduces such configurations, calculations of pure CO layers on a Ru(0001) surface were performed. Figure 3(a) shows the obtained E_{ads} values as a function of coverage. As expected, the repulsive interaction energies between the CO molecules generally increase with increasing coverage, a trend that has also been found in a previous DFT study on a smaller, $(4 \: x \: 4)$, cell.[43] The present calculations predict a spread of energies in all cases where various configurations at the same coverages were analyzed, and also predict that the ordered structures at 0.33 and 0.58 ML are more stable than the corresponding disordered structures.

7

1
2
3
4
5
6
7
8
9
10
11
12
13
14
15
16
17
18
19
20
21
22
23
24
25
26
27
28
29
30
31
32
33
34
35
36
37
38
39
40
41
42
43
44
45
46
47
48
49
50
51
52
53
54
55
56
57
58
59
60
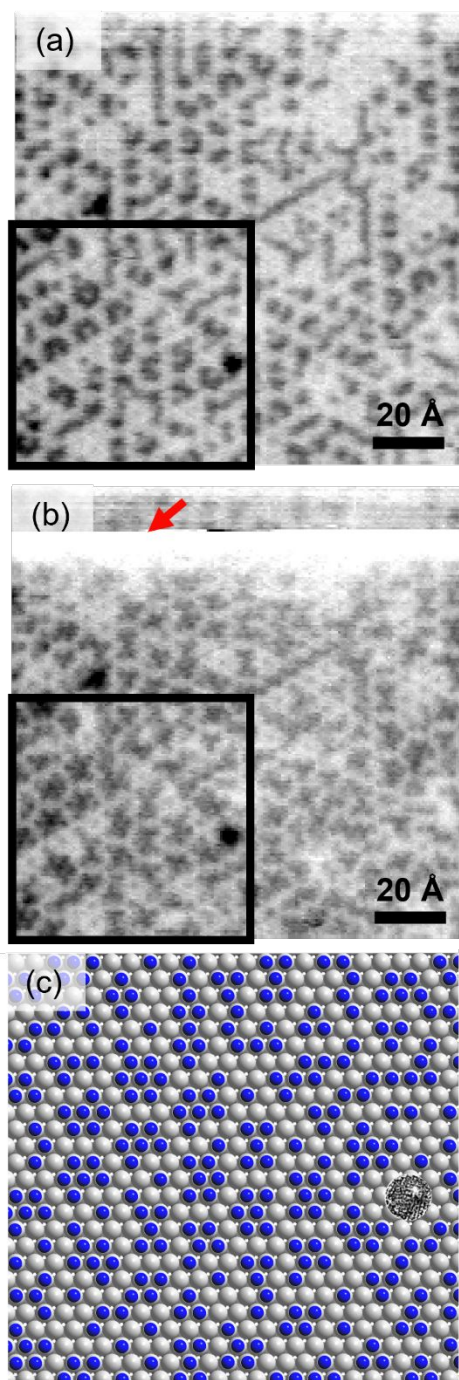
Figure 2: Effect of a tip change on the imaging contrast of the partially disordered $(2\sqrt{3}\ x\ 2\sqrt{3})R30°$ CO structure. (a) STM image recorded in the constant height mode, probably with a metallic tip (70 K, V_t = -1.00 V, I_t = 3 nA). (b) Same surface area after a tip change at the marked position (red arrow); probably the tip has an attached CO molecule. Black features represent individual CO molecules. (c) Structure model of the marked areas (black frames) in (a) and (b); CO molecules indicated in blue, Ru atoms in grey.

8
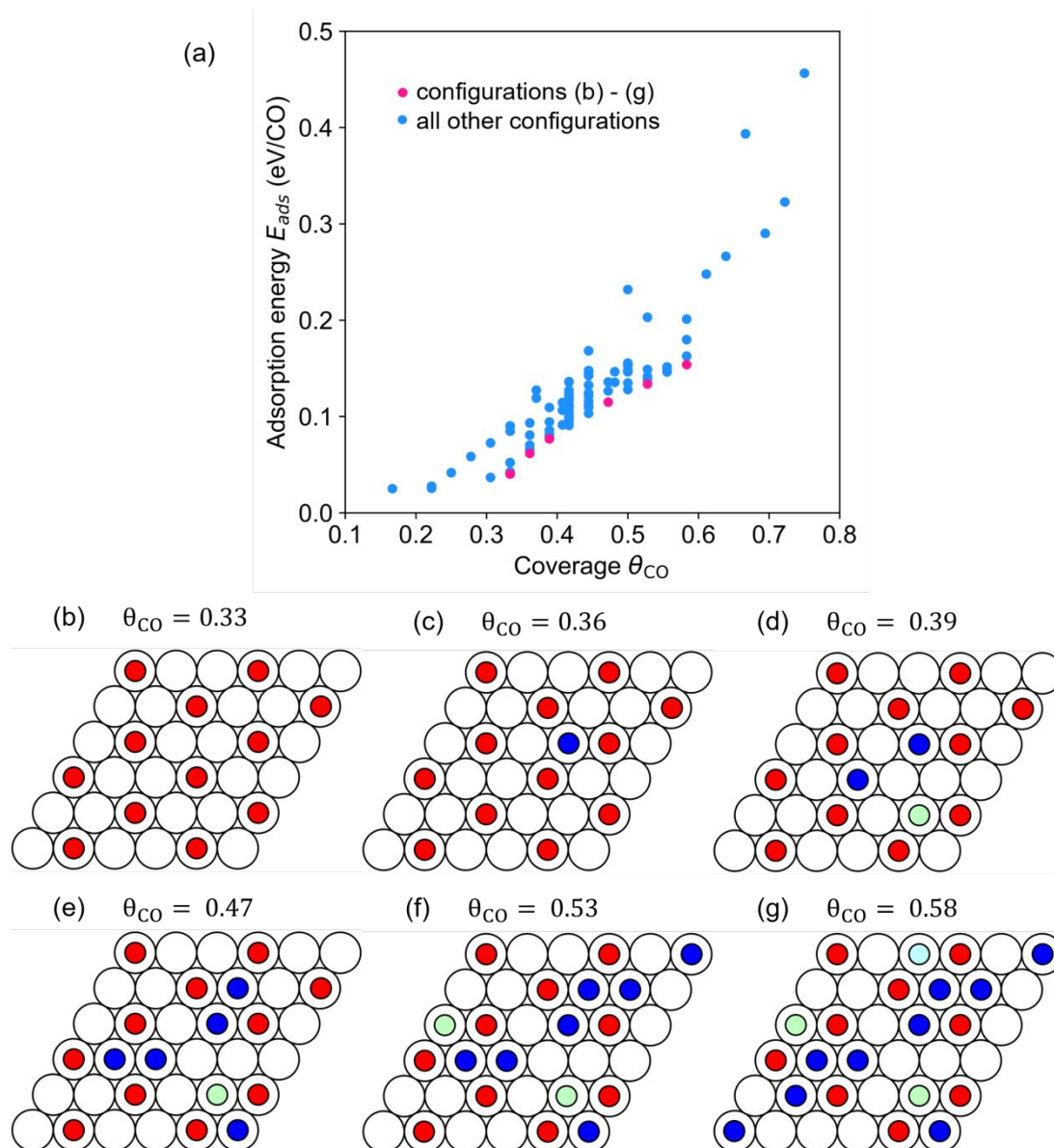
Figure 3: (a) Adsorption energies of CO relative to an isolated adsorbed CO molecule as a function of CO coverage for 105 different arrangements. (b)-(g) Energetically favorable local structures of the CO adlayer at various CO coverages. Red, blue, and green spheres represent CO molecules on $(\sqrt{3} \, x \, \sqrt{3})R30°$ sites, inserted CO molecules, and molecules displaced from $(\sqrt{3} \, x \, \sqrt{3})R30°$ sites, respectively.

For the ordered $(\sqrt{3} \, x \, \sqrt{3})R30°$ structure [figure 3 (b)] the repulsive interaction is lower than for other configurations at 0.33 ML because the distances between the molecules are maximum. When the coverage is slightly increased, the general $(\sqrt{3} \, x \, \sqrt{3})R30°$ structure is at first preserved and only locally disturbed by disordered configurations. One additional CO molecule in the $(6 \, x \, 6)$ cell is predicted to adsorb on an interstitial site in the $(\sqrt{3} \, x \, \sqrt{3})R30°$ structure [figure 3(c)].

When a second molecule is added on a neighboring interstitial site the system switches to another arrangement by pushing a CO molecule away from its $(\sqrt{3} \, x \, \sqrt{3})R30°$ lattice site. A configuration consisting of three trimers results [figure 3(d)]. This configuration effectively lowers the repulsive interactions of the disordered configuration and locally anchors the defect. Compared to configurations with two CO molecules on interstitial sites, it is by 40 meV more stable.

When the CO coverage is increased further [figures 3(e) and (f)], the layer again switches to a different type of structure that consists of partial CO rings around a central CO molecule. According to the relative energies of these structures the ring center sites are filled first, and the ring edge sites are occupied afterward. At 0.58 ML the rings are complete, and an ordered $(2\sqrt{3} \, x \, 2\sqrt{3})R30°$ structure consisting of clusters of seven molecules has formed [figure 3(g)]. At the experimental coverage of 0.47 ML, the most stable structure consists of partial rings around a center molecule [figure 3(e)]. The DFT results are thus in good agreement with the configurations observed by STM [figure 2(c)].

For the diffusion measurements, in order to ensure that the CO coverage of 0.47 ML was the same as in the preparatory experiments, the adsorption layer was prepared in the same way. After O_2 and CO adsorption, the sample was transferred to the STM and cooled to the respective temperature for the diffusion measurements.

As an example of the type of data obtained, figure 4 shows a series of 12 consecutive frames from a 3731 frames movie recorded at 271 K. (The frames are details from larger areas, and a 1296 frames section of the original data is shown in the Supplementary Information, movie S1.) The flat, grey background represents the matrix of CO molecules. The characteristic leopard skin structure is not resolved. This fact can be understood by the high mobility of the CO molecules and by the disorder of the layer at this temperature. With a calculated hopping barrier of ~0.3 eV (see below) one estimates CO hopping rates of the order of $1 - 10 \times 10^6$ Hz in the investigated temperature range. These rates are far beyond the time resolution of the fast mode of the STM, preventing imaging of the individual molecules. However, vibrational spectroscopy work has shown that the CO molecules remain at on-top sites in this temperature range, and, at least up to 300 K, no CO is lost by desorption.[40] It can therefore be assumed that the coverage and local structures are similar to those in the preparatory experiments at lower temperatures (figures 1 and 2).

In principle, the $(\sqrt{3} \, x \, \sqrt{3})R30°$ structure in the previous study was affected by similarly fast fluctuations, but there the CO matrix could be resolved well in the same range of temperatures.[11] The difference to the present data is explained by the fact that the lattice sites of the $(\sqrt{3} \, x \, \sqrt{3})R30°$ structure are minimum energy positions for the CO molecules. Interstitial positions are less favorable because of the repulsions between CO molecules on neighboring sites. The molecules rapidly jump also to these unfavorable sites but reside on $(\sqrt{3} \, x \, \sqrt{3})R30°$ lattice sites for greater fractions of time than on interstitial sites. Since the STM sees a time average of these fluctuations, a $(\sqrt{3} \, x \, \sqrt{3})R30°$ structure is resolved. By contrast, in the disordered layer at Θ_{CO} = 0.47 ML, many CO configurations are energetically equivalent, so that the time average of the fluctuations is structureless. This is in agreement with a previous LEED study according to which CO forms a fluid phase at this coverage and temperature range.[42]
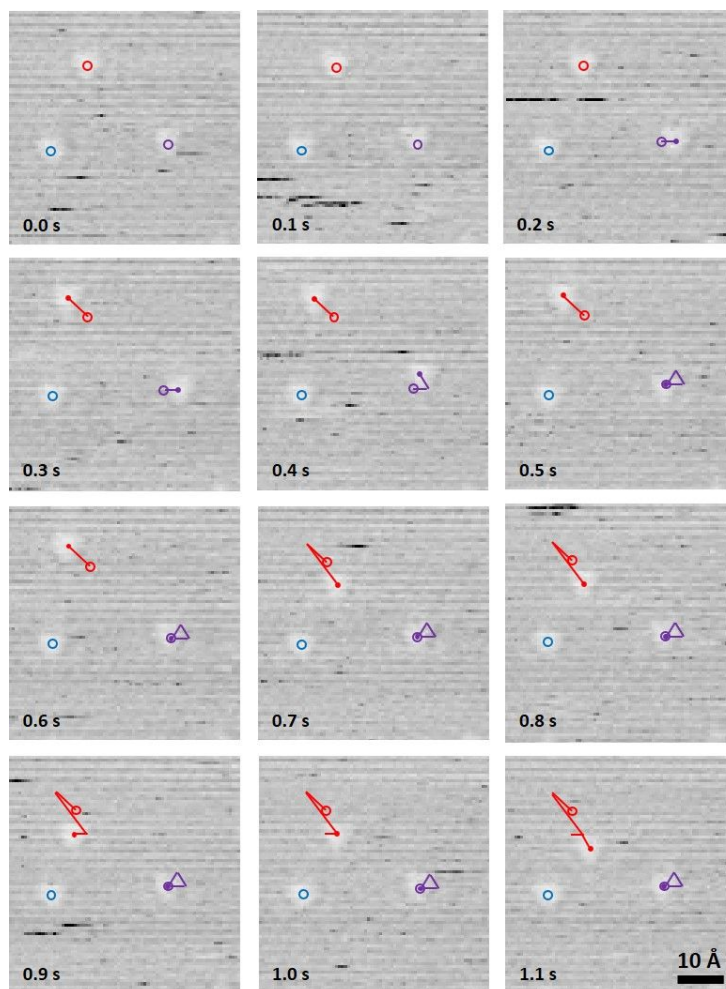
Figure 4: Hopping events of O atoms embedded in the CO layer at Θ_{CO} = 0.47 ML. The 12 frames are from a movie recorded in the constant height mode at 271 K (V_t = -0.80 V, I_t = 3 nA, 10 frames s^{-1}). The two atoms marked red and violet are O atoms, the atom marked blue is an N atom. Red and purple lines are the trajectories of the O atoms.

The three bright features in figure 4 represent two O atoms (red and violet dots) and one N atom (blue dot). O and N atoms are imaged similarly but can be distinguished by their mobilities and, in the constant current data, also by their different apparent heights.[44, 45] The right O atom (violet) has first jumped in frame 3, then again in frames 5 and 6 by approximately 3 Å, i.e., by one lattice constant of the Ru(0001) surface. The upper O atom (red) has first jumped in frame 4 by $\sqrt{3}$ lattice constants, then again in frame 8 by $2\sqrt{3}$ lattice constants, and in frames 10, 11, and 12 by one lattice constant. At 271 K the embedded O atoms are obviously mobile on the time scale of the fast mode of the STM. The N atom does not move in the entire movie, in agreement with the previously determined lower hopping rate of adsorbed N atoms on the (bare) Ru(0001) surface.[45]

For quantitative investigation, longer trajectories were analyzed by means of the tracking software.[23] Examples from measurements at 239 K and 271 K are shown in figure 5. Figure 5(a), one frame from a movie at 239 K, shows several bright atomic features most of which are identified as O atoms. (The movie is shown in the Supplementary Information, movie S2.) Some of the O atoms have formed small clusters with a (2 x 2) structure. There are also some N atoms and some smaller bright and larger dark

11

features of unknown nature, which do not move most of the time. Trajectories were only analyzed for atoms that could clearly be identified as O atoms and only for those O atoms that are sufficiently far away [> 2 Ru(0001) lattice constants] from other O atoms and other features to exclude effects of lateral interactions. When during a trajectory an O atom comes close to a second O atom or to one of the other features, the trajectory is automatically closed by the software. Usually, the trajectories are split into several coherent parts by this function.

One of the coherent trajectories of the marked O atom [figure 5(a)] is shown in figure 5(b). The time is color-coded, and the positions of the O atom identified by the tracking algorithm in successive frames are connected by lines. A hexagonal pattern appears. The lattice constant of this pattern is approximately 3 Å, i.e., within error margins, the lattice constant of the Ru(0001) surface of 2.71 Å. Directly on the lattice sites, knots consisting of shorter lines represent time periods during which the O atom is found on the same site. That the positions are not exact points is caused by the finite localization precision of the tracking algorithm.[23] The lines connecting the knots represent events in which the O atom is found on other lattice sites with respect to the previous frame. An obvious interpretation of such a trajectory is that the O atom, which occupies an hcp site on the Ru(0001) surface,[46, 47] moves across the surface by jumping between the hcp sites of the (1×1) lattice of the Ru surface. The presence of the CO matrix does not seem to change this behavior, which, qualitatively, is the same as on the empty Ru surface.[48] At a higher temperature [271 K, figure 5(c)] more lines connect the lattice sites whereas the knots contain fewer lines, indicating a higher hopping frequency, as expected. Occasional lines over $\sqrt{3}$ or two lattice constants that appear at this higher temperature must not indicate long jumps but can consist of two or more short jumps at shorter times than the time of 0.1 s for one frame of the movie.

In the $(\sqrt{3} \times \sqrt{3})R30°$ CO structure the oxygen trajectories displayed a distinctly different symmetry.[11] The oxygen positions also formed a (1×1) lattice, but when the density of lines connecting the lattice sites was considered, the pattern was not hexagonal. It displayed a superstructure of equilateral triangles, each consisting of three (1×1) sites, without shared edges and corners; figure 5(d) shows an example from a measurement at 248 K. The three corners within the triangles are connected by several lines, whereas usually only one line connects neighboring triangles. The resulting rotational symmetry is trigonal. This reduced symmetry was explained by the $(\sqrt{3} \times \sqrt{3})R30°$ structure of the CO matrix. A vacancy in this structure contains three hcp sites arranged in an equilateral triangle which can be occupied by the embedded O atom. When the O atom jumps between these three sites this does not involve a site exchange with a CO molecule and happens relatively often, explaining the high density of lines connecting the corners of the triangles. When the O atom exchanges sites with CO molecules from the matrix, this leads to a position in a neighboring triangle and happens less often, explaining the fewer lines to neighboring triangles. Such a symmetry reduction is absent here, indicating that the configuration in the vacancies of the CO matrix is different.

12
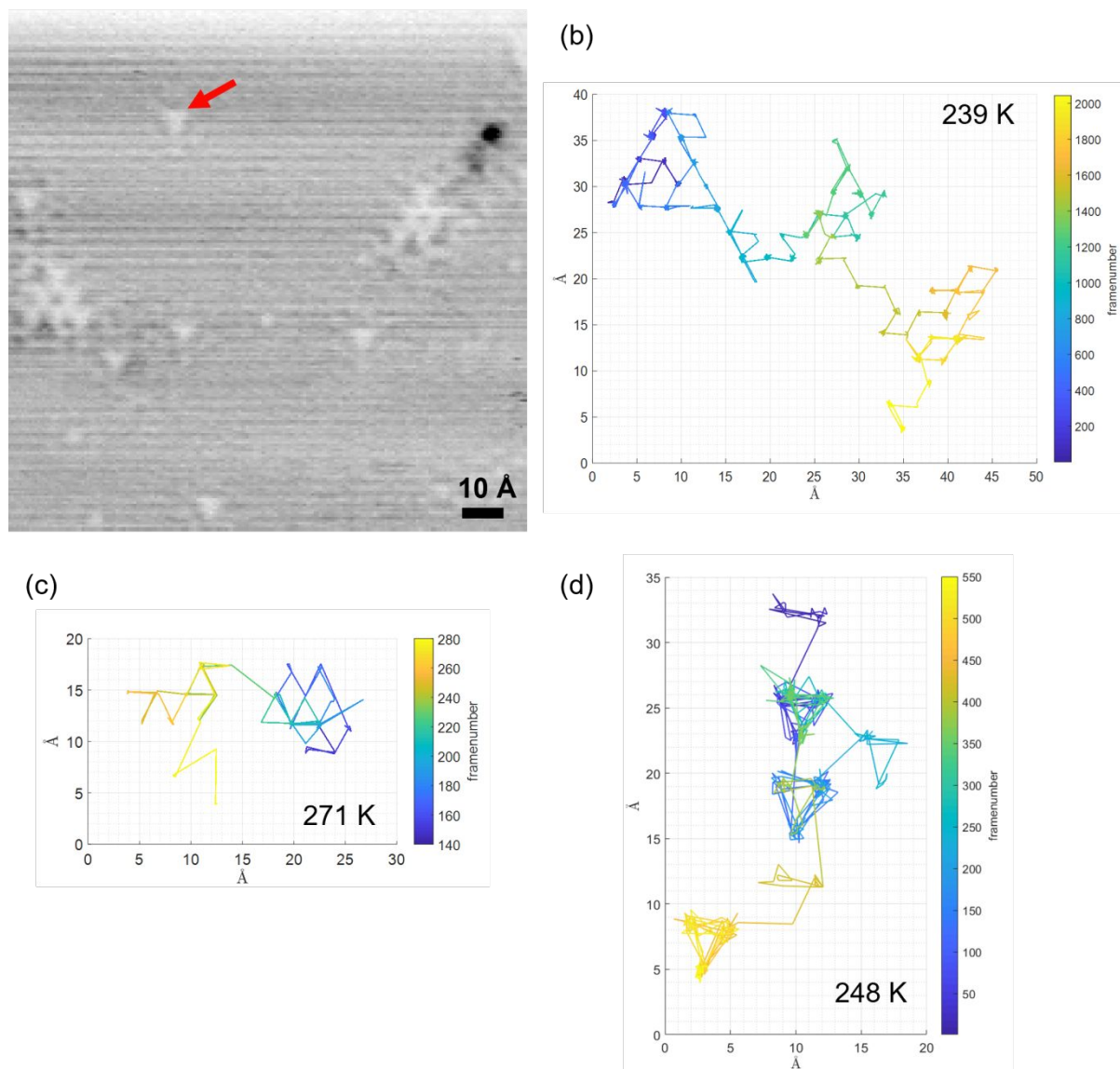
Figure 5: Trajectories of single O atoms on the Ru(0001) surface at Θ_{CO} = 0.47 ML. (a) Single frame from a movie at 239 K (V_t = -0.60 V, I_t = 3 nA, 10 frames s^{-1}). (b) Trajectory of the O atom marked in (a) by the red arrow; the time evolution is color-coded. (c) Trajectory of an O atom from an experiment at 271 K (V_t = -0.80 V, I_t = 3 nA, 10 frames s^{-1}). (d) Trajectory of an O atom from an experiment at Θ_{CO} = 0.33 ML at 248 K (V_t = -0.22 V, I_t = 3 nA, 10 frames s^{-1}).

13

The hopping statistics from all trajectories at Θ_{CO} = 0.47 ML, recorded at 239 K, 247 K, 258 K, 271 K, and 280 K, are collected in the histograms of figures 6(a) to (e) (magenta bars). Each histogram is a displacement distribution $P_{t_0}(x,y)$, which represents the probability that an O atom detected in one frame of a movie is displaced by a vector (x,y) from its position in the preceding frame, defined as $(0,0)$ [the components of the vector (x,y) are in units of the (1×1) lattice of the Ru(0001) surface]. In all cases, the probability of finding the atom at the same site, i.e., at $(0,0)$ is highest, and the probabilities of finding it at nearest neighbor, next-nearest neighbor, etc., (1×1) sites decrease with distance from the origin. This is the expected behavior for diffusional motion. With increasing temperature, the central bar becomes lower and the bars at longer distances increase. All histograms display hexagonal symmetry, confirming, with high statistical significance, the qualitative impression from the trajectories that the jumps happen uniformly in the six equivalent directions of the (1×1) lattice. By contrast, the histograms obtained in the previous study on the $(\sqrt{3} \times \sqrt{3})R30°$ structure clearly reflected the trigonal symmetry of the trajectories.[11]

To analyze these data a model was used that has originally been constructed for STM data of the diffusion of O atoms on the bare Ru(0001) surface,[48] and, in similar form, for field-ion microscopy (FIM) data of adsorbed metal atoms.[49] The model assumes that the jumps of an O atom are statistically uncorrelated. It furthermore assumes that only jumps to neighboring (1×1) sites occur, and that they happen with the same probability in the six equivalent directions of the lattice. Memory effects in successive jumps and long jumps are ruled out. When these assumptions are fulfilled, a displacement distribution $P_{t_0}(x,y)$ is predicted that can be expressed as a sum over a product of two terms

$$P_{t_0}(x,y) = \sum_{n=0}^{\infty} \tilde{P}_{t_0}(n) \cdot w_n(x,y)$$

$\tilde{P}_{t_0}(n)$, the first term in this product, is the probability that the O atom jumps n times between two successive frames of a movie. The model does thus not assume that every jump event is resolved but it allows for arbitrary many jumps between two frames. This probability is given by a Poisson distribution

$$\tilde{P}_{t_0}(n) = \frac{(\Gamma t_0)^n}{n!}e^{-\Gamma t_0}$$

Γ is the jump frequency, the inverse of the average time the atom resides on an adsorption site. t_0 is the time interval of the Poisson distribution, which in the present case is given by the time for one STM frame, and n is the number of hopping events in this time interval.

The second term in the product, $w_n(x,y)$, is the probability that an O atom located at $(0,0)$ in one frame has travelled to a site (x,y) in the following frame by a combination of n jumps. This factor only depends on the lattice symmetry, i.e., in the present case, on the hexagonal (1×1) lattice of hcp sites on the Ru surface. $w_n(x,y)$ is evaluated by means of the recursion equation

$$w_n(x,y) = \sum_{x',y'} \frac{1}{6}w_{n-1}(x',y')$$

14
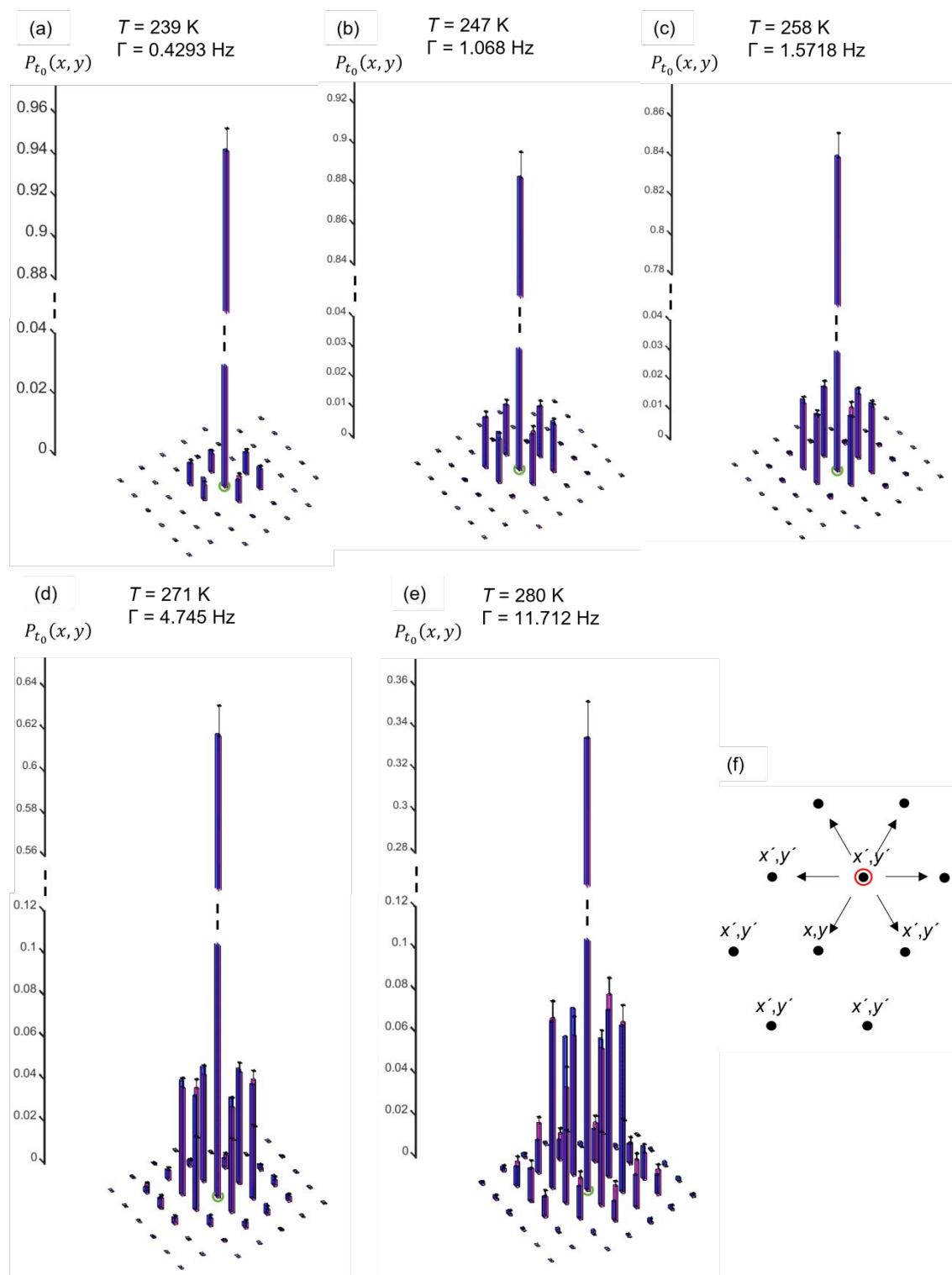
Figure 6: (a)-(e) Displacement histograms of an embedded O atom at five different temperatures at Θ_{CO} = 0.47 ML. The bars represent the probabilities that the atom has jumped from the lattice site (0,0) in the center of the indicated lattice section (green marks) to one of the lattice sites between two successive frames. Magenta bars are experimental data from the STM movies, blue bars are fits based on the model described in the text. The negative going error bars are not shown for clarity; they are identical to the indicated positive going error bars. (f) Lattice sites used in the recursion equation. The red circle marks an O atom that has travelled to one of the nearest-neighbor lattice sites (x',y') of the site (x,y) by $(n-1)$ jumps; the arrows indicate the directions into which it can jump by the nth jump.

15

The positions (x',y') in this equation are the coordinates of the six nearest-neighbor sites around the site (x,y) [figure 6(f)]. The equation expresses the fact that an atom that has travelled to one of the sites (x',y') by $(n-1)$ jumps has a chance of 1/6 to jump to the site (x,y) by the n's jump. The five other, equally likely, jumps from the given site (x',y') land on other sites [figure 6(f)]. Adding these probabilities over the six nearest-neighbor sites (x',y') around (x,y) gives $w_n(x,y)$. The recursion equation makes use of the assumption of the model that jumps only occur over one lattice constant and happen with the same probability in the six equivalent directions of the lattice. The recursion is initialized by setting $w_0(0,0) = 1$ and all other $w_0(x,y) = 0$. n is then increased in steps of unity to calculate sets of $w_n(x,y)$ values for the various sites (x,y).

Multiplying the spatial factor $w_n(x,y)$ by the time factor $\tilde{P}_{t_0}(n)$ and adding over all n finally gives $P_{t_0}(x,y)$. Practically, the infinite sum over n can be terminated at a sufficiently high number; in this case we chose n = 10. [The analogue analysis for the $(\sqrt{3}\,x\,\sqrt{3})R30°$ CO structure was considerably more complicated because of the two different hopping processes involved.[11]]

The only unknown in the resulting expression for $P_{t_0}(x,y)$ is the hopping rate Γ. Γ can therefore be evaluated by fitting $P_{t_0}(x,y)$ to the experimental $P_{t_0}(x,y)$ histograms. The resulting fits are also shown in figures 6(a) to (e) (blue bars). The agreement with the experimental values is very good, as one can also see in the residual plots (Supplementary Information, figure S1). Obviously, the CO molecules may affect the O atoms by changing the average hopping rate, but they do not influence the lengths and directions of the jumps or the fact that the jumps are statistically uncorrelated.

The data sets at the five analyzed temperatures provide a set of temperature-dependent hopping rates $\Gamma(T)$. Figure 7 shows an Arrhenius plot of these data (red crosses). A linear regression line gives a good fit (red line), from the slope of which an activation energy of $E^* = 0.44 \pm 0.04$ eV is obtained and from the intercept a preexponential factor of $\Gamma^0 = 10^{8.9 \pm 0.8}$ s^{-1}. The low preexponential factor most likely results from the fact that only five data points are available. When we fix the preexponential factor at the mean value $\Gamma^0 = 10^{11.2}$ s^{-1} obtained with the higher number of data points at Θ_{CO} = 0.33 ML, an activation energy of $E^* = 0.56 \pm 0.04$ eV is obtained (red dotted line).

In the same Arrhenius plot we also show the data from the previous investigation of the diffusion of O atoms through the $(\sqrt{3}\,x\,\sqrt{3})R30°$ CO structure at Θ_{CO} = 0.33 ML.[11] As mentioned above, this process involves two steps, jumps of the O atoms within the triangular vacancies of the CO layer without site exchanges with CO molecules (shown as blue points in the figure), and exchange jumps with neighboring CO molecules (shown as green points). Site exchanges with CO molecules are slower than jumps to the empty sites within the triangular vacancies. The activation energies obtained were $E_1^* = 0.57 \pm 0.02$ eV and $E_2^* = 0.63 \pm 0.03$ eV for the triangular and the exchange jumps, respectively, in good agreement with the DFT-calculated values; the preexponential factors were $\Gamma_1^0 = 10^{11.4 \pm 0.4}$ s^{-1} and $\Gamma_2^0 = 10^{11.1 \pm 0.7}$ s^{-1}, close to the expected range of 10^{12} - 10^{13} s^{-1}.

16
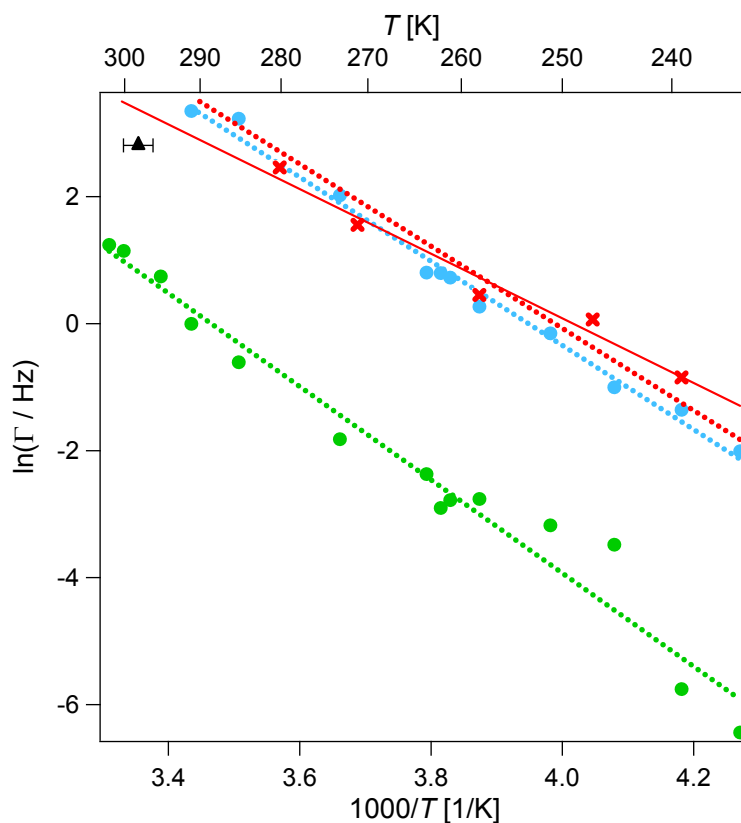
Figure 7: Arrhenius plot of the hopping frequencies of the embedded O atoms. Red crosses: Data points from the present study at Θ_{CO} = 0.47 ML; the solid red line is a linear regression; the dotted red line is a linear regression with a preexponential factor fixed at $\Gamma^0 = 10^{11.2}$. Green dots: Data points from the jumps of the O atoms in the triangular vacancies at Θ_{CO} = 0.33 ML; blue dots: Data points from the exchange jumps with CO molecules at Θ_{CO} = 0.33 ML.[11] The 0.33 ML data are adapted with permission from ref.[11]; copyright 2019 American Association for the Advancement of Science. Black triangle: Hopping rate of an O atom on the bare Ru(0001) surface at room temperature.[50]

At the higher coverage in the present study, the motion of the O atoms through the CO layer necessarily involves site exchanges with CO. It is therefore quite surprising that the hopping rates (red crosses) are higher than the exchange jumps at the lower coverage (green points). The hopping rates at 0.47 ML almost coincide with the rates of the triangular jumps from the data at Θ_{CO} = 0.33 ML that do not involve sites exchanges with CO (blue points). Moreover, when one extrapolates the regression lines (both of them) through the 0.47 ML data points to 300 K one finds that the hopping rate is even somewhat higher than the hopping rate of O atoms on the bare Ru(0001) surface measured at room temperature (black triangle).[50]

Figures 8 and 9 show results of the DFT calculations performed to explain these observations. A general result is that, in the presence of the O atom, the E_{ads} values are higher [figure 8(a)] than for the pure CO layers [figure 3(a)], i.e., the repulsive interactions between O and CO are higher than between the CO molecules. This is in agreement with previous findings of a weaker binding of CO on an interstitial site in the (2×2)O structure.[51] Figures 8(b) - (g) show how these interactions affect the configurations around the O atom. In all cases the O atom occupies an hcp site. The three Ru atoms forming the hcp site are blocked for the binding of CO, which leads to a vacancy in the CO layer.

17
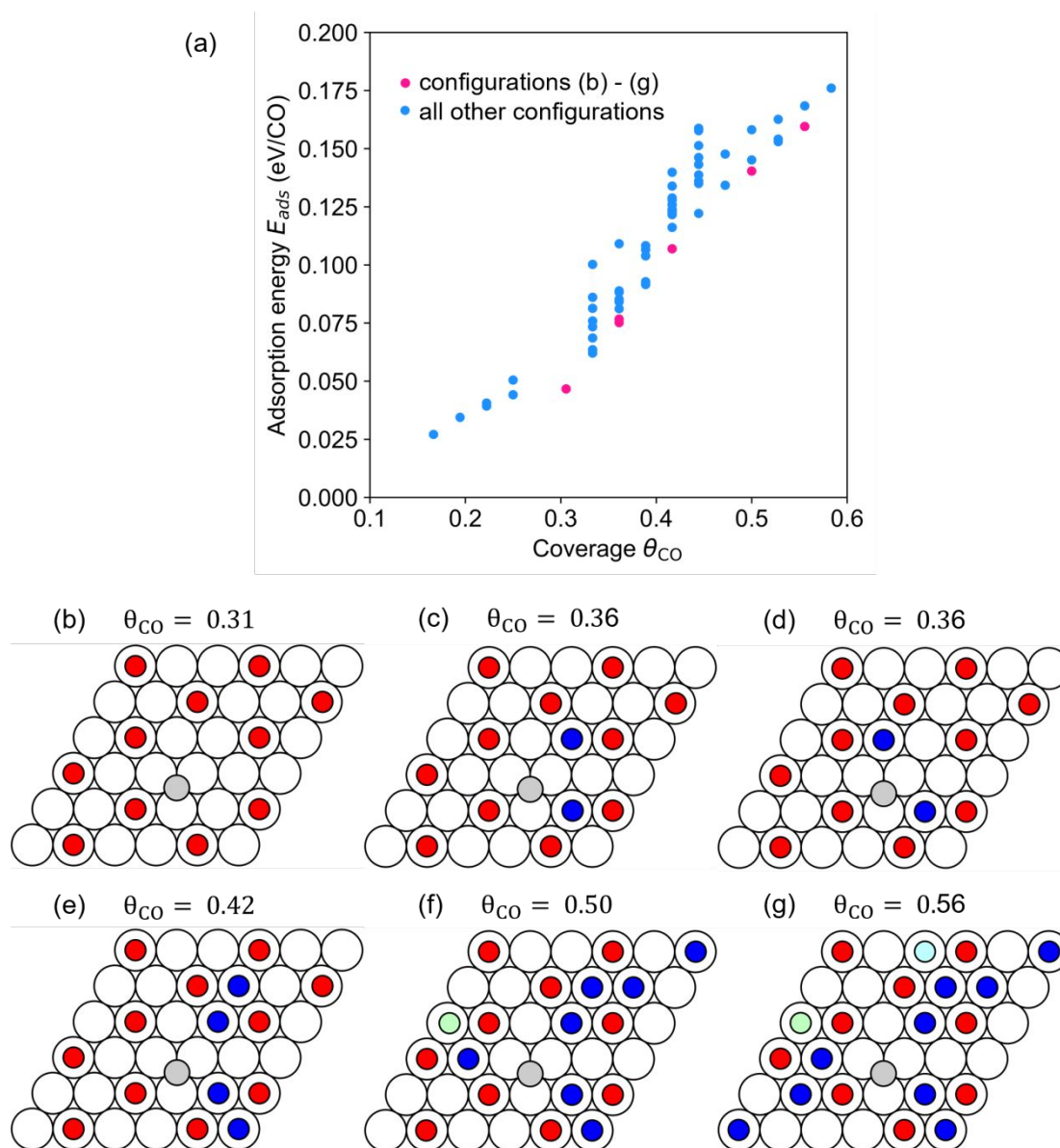
Figure 8: (a) Adsorption energies of CO relative to an isolated adsorbed CO molecule in the presence of one coadsorbed O atom as a function of CO coverage for 85 different arrangements. (b)-(g) Energetically favorable CO arrangements around an O atom (grey sphere) at increasing CO coverages. Red, blue, and green spheres represent CO molecules on $(\sqrt{3} \, x \, \sqrt{3})R30°$ sites, inserted CO molecules, and molecules displaced from $(\sqrt{3} \, x \, \sqrt{3})R30°$ sites, respectively.

Which configuration is formed inside the vacancy depends on the CO coverage. At a coverage close to 0.33 ML, where the CO layer forms the $(\sqrt{3} \, x \, \sqrt{3})R30°$ structure [figure 8(b), Θ_{CO} = 0.31 ML], six CO molecules form a relatively large cage around the O atom. The cage contains three hcp sites that can be occupied by the O atom, and jumps between these sites caused the fast triangular motion at this coverage.[11] When the coverage is increased, one CO molecule intrudes into the cage, and at Θ_{CO} = 0.36 ML two CO molecules have intruded [figures 8(c) and (d)]. Both molecules form trimer configurations with CO molecules at the rim of the cage, the same trimers as in the pure CO layer at moderately increased coverages [figure 3(d)]. Despite the presence of the O atom, the configuration

with two CO molecules inside the cage is by 0.13 eV more stable than when the molecules are put on interstitial sites in the $(\sqrt{3} \times \sqrt{3})R30°$ layer outside the cage (not shown).

When the CO coverage is increased further – figures 8(e), (f), and (g) show optimized configurations at Θ_{CO} = 0.42, 0.50, and 0.56 ML – the additional CO molecules adsorb in the CO layer outside the cage. There they form the same filled-ring structures as in the pure CO layer [figures 3(e) - (g)], whereas the configuration with two intruded CO molecules inside the cage remains unchanged. The cage is smaller than at 0.33 ML, which has consequences for the mobility of the O atom. In order to jump, the O atom needs a suitable target site, a neighboring hcp site which is completely free of CO molecules. The two intruded CO molecules effectively block these target sites within the cage. Consequently, triangular jumps do no longer occur in the coverage range between 0.36 and 0.56 ML, in agreement with the absence of triangles in the trajectories recorded at 0.47 ML.

However, the O atom can move when the CO molecules at the rim of the cage are intermediately displaced. For the calculations, determining preferred local configurations during such processes is made difficult by the many, almost degenerate possibilities to arrange the CO molecules. What simplifies the problem is the fact that the local structures within the cage are independent of coverage between 0.36 and 0.56 ML and that the target site always has to be an empty hcp site.

We therefore focus on one particular configuration for which we analyze several scenarios [Figure 9(a) – (c), Θ_{CO} = 0.36 ML]. In the first scenario [figure 9(a)], at first the more distant of the two CO molecules in the cage moves from a trimer site to an interstitial site. This step, which has an activation energy of 0.33 eV and increases the ground state energy by 0.06 eV, creates an empty hcp site. Then the O atom can jump, which happens in two steps, first to an intermediate fcc site with an activation energy of 0.61 eV, and then to the empty hcp site with an activation energy of 0.65 eV (both activation energies are with respect to the initial configuration). In the other two scenarios [figures 9(b) and (c)], one of the CO molecules at the rim of the original cage moves first, connected with activation energies of 0.25 and 0.29 eV, and with 0.11 and 0.15 eV higher ground state energies, respectively. The jumps of the O atom via the intermediate fcc sites are connected with activation energies of 0.66/0.73 eV and 0.71/0.67 eV, respectively. The last configurations in figure 9 all have higher energies than the initial configurations, but subsequent rearrangement processes in the CO layer can restore the original ground state energy. Because the CO jumps have activation energies of only ~0.3 eV, these processes are very fast in the considered temperature range. In the final configurations, the O atom has, in effect, performed a site exchange with a CO molecule.

Note that the activation energies of the initial CO displacements do not contribute to the total activation energies. In kinetics terms, these very fast first steps represent preequilibria to the actual O hopping that only contribute by increasing the ground state energies [e.g., by 0.06 eV in figure 9(a)]. The total activation energy values given in figure 9 contain these initial increases.
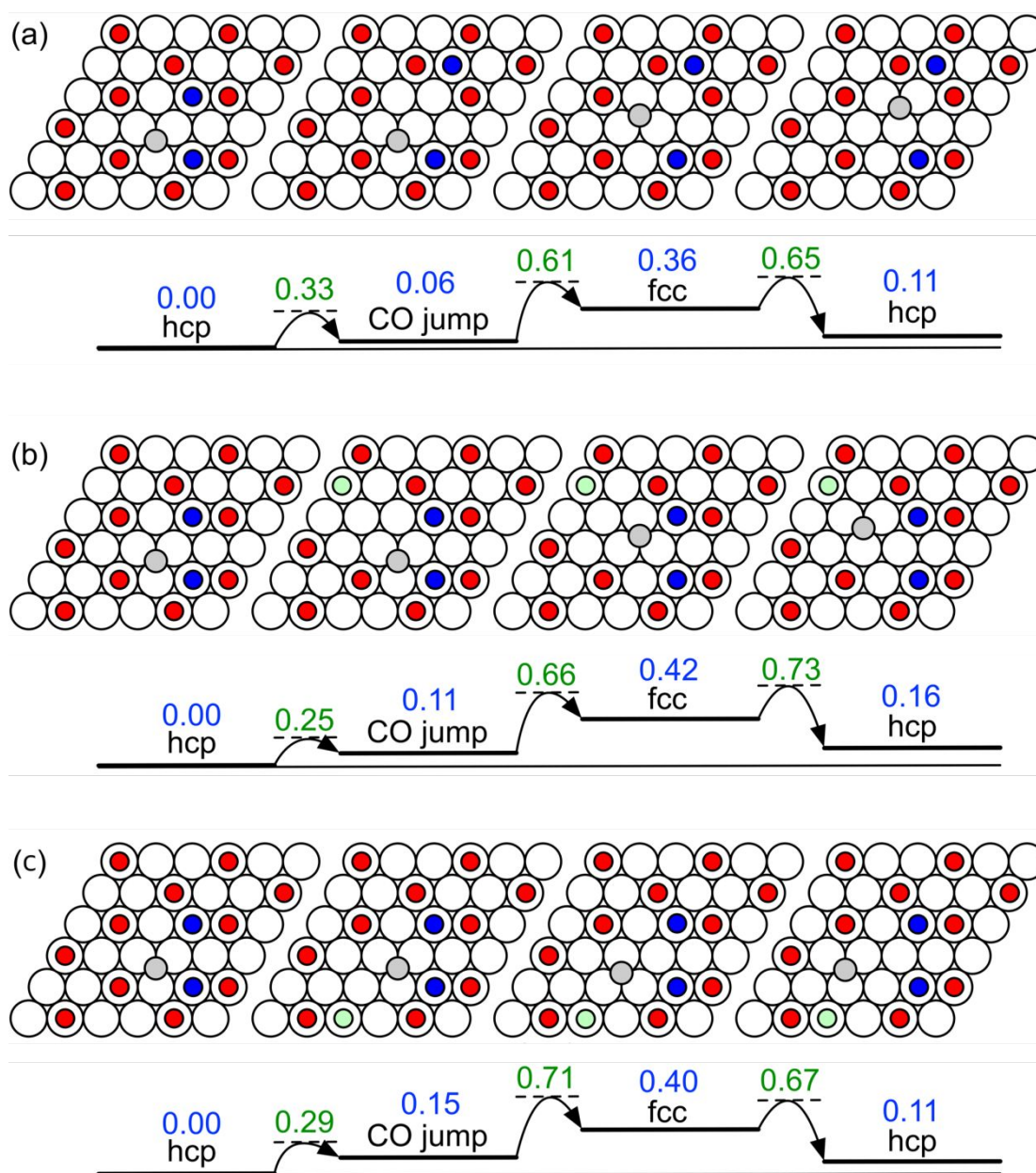
Figure 9: Hopping mechanisms of an O atom with two CO molecules in the cage. (a) – (c) Three different scenarios starting from the same configuration. The grey sphere represents an O atom. Red, blue, and green spheres represent CO molecules on $(\sqrt{3} \, x \, \sqrt{3})R30°$ sites, inserted CO molecules, and molecules displaced from $(\sqrt{3} \, x \, \sqrt{3})R30°$ sites, respectively. The energy profiles are indicated below the configurations.

All total activation energies are lower than the values calculated for the O/CO exchange on the $(\sqrt{3} \, x \, \sqrt{3})R30°$ structure (0.78/0.71 eV with respect to the initial configuration).[11] There are two reasons for this. First, at the higher coverage, scenarios are possible, in which the first displacement of a CO molecule costs less energy than for the $(\sqrt{3} \, x \, \sqrt{3})R30°$ structure. For example, in figure 9(a) the ground state energy only increases by 0.06 eV, compared to 0.16 eV for the $(\sqrt{3} \, x \, \sqrt{3})R30°$ structure.[11] This reduction results from the fact that at the higher coverage the CO molecules already occupy unfavorable sites, so that a displacement has a smaller effect. Second, for the jump of the O atom, after the initial displacement of a CO molecule, the starting position is already energetically uplifted with respect to the $(\sqrt{3} \, x \, \sqrt{3})R30°$ structure because the O atom is coordinated to more CO

20

molecules. At the same time, the transition state, roughly the bridge site between the hcp and the fcc sites, is less affected by CO because the distances to the neighboring CO molecules are larger. In effect, the barrier is lowered. Moreover, in the experiment, the scenario with the lowest barrier contributes disproportionally strongly because the barrier appears exponentially in the Arrhenius equation.

At 0.47 ML, the local configurations are more complicated and require more CO jumps to open a diffusion path. However, because of the low activation energies of the CO jumps of ~0.3 eV these processes are fast and not rate-limiting. For the ground states many initial fluctuations in the ring-like CO clusters are even energetically neutral. The activation energy is therefore reduced further, which should bring it close to the value calculated for the triangular jumps in the cages of the $(\sqrt{3} \, x \, \sqrt{3})R30°$ structure (0.56 eV).[11] The experimental finding that the exchange jumps at the higher coverage are similarly fast as the triangular jumps at 0.33 ML (figure 7) can thus be understood. That the jump rate is even somewhat faster than on the bare metal surface is caused by the repulsion between O and CO. Finally, with regard to symmetry, the individual CO configurations in figure 9 only have low symmetries. However, as the experiment averages over many possible, quickly fluctuating CO configurations, the overall symmetry of the displacement histograms is hexagonal (figure 6).

The enhanced mobility of the O atom at the higher CO coverage is thus the result of a higher probability of fluctuations in the CO layer and of an enhanced repulsion between the O atom and the CO molecules. The former aspect is supported by previous experiments on the mobility of adsorbed CO on Ru(0001) using laser-induced thermal desorption (LITD).[52] With this method a macroscopic CO self-diffusion constant was measured that increased with CO coverage. This may appear counterintuitive at first but is in good agreement with the interpretation of the present data.

Conclusions

In this study, individual adsorbed O atoms on a Ru(0001) surface in a dense layer of CO molecules were investigated by STM. The CO coverage of approximately 0.47 ML was higher than in a previous study on the ordered $(\sqrt{3} \, x \, \sqrt{3})R30°$ structure at 0.33 ML, and the layer was disordered.

High-speed STM experiments on the diffusion of the O atoms through the CO layer show that certain features of the diffusion mechanism are the same as in the previous study, but that there are also marked differences. Similarly as at the lower coverage, the O atoms move by statistically uncorrelated jumps, and they only hop between nearest neighbor hcp sites on the $(1 \, x \, 1)$ lattice of the Ru(0001) surface. Differently from the lower coverage, the motion of the O atoms only consists of one type of jump and the jumps occur with the same probability into the six equivalent directions of the $(1 \, x \, 1)$ lattice. In the previous study a combination of two different jump types was required to describe the data. A second difference is that the jump frequency, which involves exchange processes of the O atom with CO molecules, is significantly higher than the O/CO exchange processes on the $(\sqrt{3} \, x \, \sqrt{3})R30°$ structure.

The DFT calculations performed in this study explain these observations. They show that the vacancy in the CO layer, a cage occupied by the O atom, is smaller at the enhanced coverage, suppressing the motion within the cage that caused the second type of jumps at the lower coverage. Fluctuations in the surrounding disordered CO layer cost less energy than at the lower CO coverage or are even energetically neutral. Configurations in which the O atom can leave the cage are therefore more likely. Moreover, the enhanced repulsion between the O atom and the CO molecules at the higher coverage lowers the activation energy for the jumps.

In detail, the atomic steps underlying the motion of the O atom through the CO layer are different from those at the lower coverage. However, like at the lower coverage, the O atom can only move through the CO layer when the cage of neighboring CO molecules opens by a local fluctuation. The door-opening mechanism is therefore still operative.

The situation investigated here, relatively strongly bound particles moving through a disordered layer of mobile molecules, should be characteristic for many catalytic reactions at the usually employed high pressures and temperatures. The mechanism may therefore play a more general role in catalysis. An example is the cobalt-catalyzed Fischer-Tropsch synthesis, an industrial process by which hydrocarbons are formed from mixtures of CO and H_2. According to the often-assumed reaction mechanism, the reaction is initiated by the dissociation of CO molecules on the metal surface.[53] C and O atoms are formed in an adsorption layer that mainly consists of CO molecules, leading to a situation similar to the one analyzed here. Even the CO coverages are comparable - for a Co(0001) model catalyst coverages between approximately 0.4 and 0.5 ML have been predicted for industrial reaction conditions - and the layer is also disordered.[54] We therefore predict that the surface diffusion of the O and C atoms in this reaction should not be restricted by the CO layer.

22

1
2
3
4
5
6
7
8
9
10
11
12
13
14
15
16
17
18
19
20
21
22
23
24
25
26
27
28
29
30
31
32
33
34
35
36
37
38
39
40
41
42
43
44
45
46
47
48
49
50
51
52
53
54
55
56
57
58
59
60

Supplementary Information

STM movie of single oxygen atoms in a CO adlayer at 0.47 ML and 271 K (AVI)

STM movie of single oxygen atoms in a CO adlayer at 0.47 ML and 239 K (AVI)

Residual plots of the displacement histograms of figure 6

Acknowledgements

23

References

1.   van Santen, R. A.; Niemantsverdriet, J. W., *Chemical kinetics and catalysis*. Plenum Press: New York and London, 1995.

2.   Stoltze, P., Microkinetic simulation of catalytic reactions. *Prog. Surf. Sci.* **2000,** *65*, 65-150.

3.   Motagamwala, A. H.; Ball, M. R.; Dumesic, J. A., Microkinetic Analysis and Scaling Relations for Catalyst Design. *Annu. Rev. Chem. Biomol. Eng.* **2018,** *9*, 413-450.

4.   Nilekar, A. U.; Greeley, J.; Mavrikakis, M., A Simple Rule of Thumb for Diffusion on Transition-Metal Surfaces. *Angew. Chem. Int. Ed.* **2006,** *45*, 7046-7049.

5.   Mak, C. H.; Koehler, B. G.; Brand, J. L.; George, S. M., Surface diffusion of hydrogen on carbon-covered Ru(001) surfaces studied using laser-induced thermal desorption. *J. Chem. Phys.* **1987,** *87*, 2340-2345.

6.   Brand, J. L.; Deckert, A. A.; George, S. M., Surface diffusion of hydrogen on sulfur-covered Ru(001) surfaces studied using laser-induced thermal desorption. *Surf. Sci.* **1988,** *194*, 457-474.

7.   Mak, C. H.; Deckert, A. A.; George, S. M., Effects of coadsorbed carbon monoxide on the surface diffusion of hydrogen on Ru(001). *J. Chem. Phys.* **1988,** *89*, 5242-5250.

8.   Xiao, X.-D.; Xie, Y.; Jakobsen, C.; Galloway, H.; Salmeron, M.; Shen, Y. R., Impurity Effect on Surface Diffusion: CO/S/Ni(110). *Phys. Rev. Lett.* **1995,** *74*, 3860-3863.

9.   Westre, E. D.; Brown, D. E.; Kutzner, J.; George, S. M., Surface diffusion of carbon monoxide and potassium coadsorbed on Ru(001): Confirmation of a 1:1 CO:K trapping interaction. *J. Chem. Phys.* **1996,** *104*, 7313-7324.

10.   Zhao, W.; Asscher, M., Coverage grating template for the study of surface diffusion: K coadsorbed with CO on Re(001). *Surf. Sci.* **1999,** *429*, 1-13.

11.   Henß, A.-K.; Sakong, S.; Messer, P. K.; Wiechers, J.; Schuster, R.; Lamb, D. C.; Groß, A.; Wintterlin, J., Density fluctuations as door-opener for diffusion on crowded surfaces. *Science* **2019,** *363*, 715-718.

12.   Sakong, S.; Henß, A.-K.; Wintterlin, J.; Groß, A., Diffusion on a Crowded Surface: kMC Simulations. *J. Phys. Chem. C* **2020,** *124*, 15216-15224.

13.   Mehrer, H., *Diffusion in Solids*. 1 ed.; Springer-Verlag: Berlin Heidelberg, 2007.

14.   van Gastel, R.; Somfai, E.; van Saarloos, W.; Frenken, J. W. M., A giant atomic slide puzzle. *Nature* **2000,** *408*, 665.

15.   van Gastel, R.; Somfai, E.; van Albada, S. B.; van Saarloos, W.; Frenken, J. W. M., Nothing Moves a Surface: Vacancy Mediated Surface Diffusion. *Phys. Rev. Lett.* **2001,** *86*, 1562-1565.

16.   Grant, M. L.; Swartzentruber, B. S.; Bartelt, N. C.; Hannon, J. B., Diffusion Kinetics in the Pd/Cu(001) Surface Alloy. *Phys. Rev. Lett.* **2001,** *86*, 4588-4591.

17.   Hsieh, M.-F.; Lin, D.-S.; Tsay, S.-F., Possibility of direct exchange diffusion of hydrogen on the Cl/Si(100)-2x1 surface. *Phys. Rev. B* **2009,** *80*, 045304.

18.   Rahn, B.; Wen, R.; Deuchler, L.; Stremme, J.; Franke, A.; Pehlke, E.; Magnussen, O. M., Coadsorbate-Induced Reversal of Solid-Liquid Interface Dynamics. *Angew. Chem. Int. Ed.* **2018,** *57*, 6065-6068.

19.   Henß, A. K.; Wiechers, J.; Schuster, R.; Platschkowski, V.; Wintterlin, J., A beetle-type, variable-temperature scanning tunneling microscope for video-rate imaging. *Jpn. J. Appl. Phys.* **2020,** *59*, SN1007.

20.   van Staden, M. J.; Roux, J. P., The superposition of carbon and ruthenium auger spectra. *Appl. Surf. Sci.* **1990,** *44*, 259-262.

21.   Marchini, S.; Günther, S.; Wintterlin, J., Scanning tunneling microscopy of graphene on Ru(0001). *Phys. Rev. B* **2007,** *76*, 075429.

24

22.	Goodman, D. W.; White, J. M., Measurement of active carbon on ruthenium (110): Relevance to catalytic methanation. *Surf. Sci.* **1979,** *90*, 201-203.

23.	Messer, P. K.; Henß, A. K.; Lamb, D. C.; Wintterlin, J., A multiscale wavelet algorithm for atom tracking in STM movies. *New J. Phys.* **2022,** *24*, 033016.

24.	Kresse, G.; Furthmüller, J., Efficient iterative schemes for ab initio total-energy calculations using a plane-wave basis set. *Phys. Rev. B* **1996,** *54*, 11169-11186.

25.	Hammer, B.; Hansen, L. B.; Nørskov, J. K., Improved adsorption energetics within density-functional theory using revised Perdew-Burke-Ernzerhof functionals. *Phys. Rev. B* **1999,** *59*, 7413-7421.

26.	Blöchl, P. E., Projector augmented-wave method. *Phys. Rev. B* **1994,** *50*, 17953-17979.

27.	Grimme, S.; Antony, J.; Ehrlich, S.; Krieg, H., A consistent and accurate ab initio parametrization of density functional dispersion correction (DFT-D) for the 94 elements H-Pu. *J. Chem. Phys.* **2010,** *132*, 154104.

28.	Grimme, S., Density functional theory with London dispersion corrections. *Wiley Interdiscip. Rev.-Comput. Mol. Sci.* **2011,** *1*, 211-228.

29.	Sakong, S.; Forster-Tonigold, K.; Groß, A., The structure of water at a Pt(111) electrode and the potential of zero charge studied from first principles. *J. Chem. Phys.* **2016,** *144*, 194701.

30.	Sakong, S.; Groß, A., The Importance of the Electrochemical Environment in the Electro-Oxidation of Methanol on Pt(111). *ACS Catal.* **2016,** *6*, 5575-5586.

31.	Mahlberg, D.; Sakong, S.; Forster-Tonigold, K.; Groß, A., Improved DFT Adsorption Energies with Semiempirical Dispersion Corrections. *J. Chem. Theory Comput.* **2019,** *15*, 3250-3259.

32.	Madey, T. E.; Menzel, D., Adsorption of CO on (001) Ruthenium at Temperatures ≥ 300 K. *Jpn. J. Appl. Phys.* **1974,** *13*, 229.

33.	Pfnür, H.; Feulner, P.; Menzel, D., The influence of adsorbate interactions on kinetics and equilibrium for CO on Ru(001). II. Desorption kinetics and equilibrium. *J. Chem. Phys.* **1983,** *79*, 4613-4623.

34.	Henkelman, G.; Jónsson, H., Improved tangent estimate in the nudged elastic band method for finding minimum energy paths and saddle points. *J. Chem. Phys.* **2000,** *113*, 9978-9985.

35.	Chen, Q.; Liu, J.; Zhou, X.; Shang, J.; Zhang, Y.; Shao, X.; Wang, Y.; Li, J.; Chen, W.; Xu, G.; Wu, K., Unveiling Structural Evolution of CO Adsorption on Ru(0001) with High-Resolution STM. *J. Phys. Chem. C* **2015,** *119*, 8626-8633.

36.	Lechner, B. A. J.; Feng, X.; Feibelman, P. J.; Cerdá, J. I.; Salmeron, M., Scanning Tunneling Microscopy Study of the Structure and Interaction between Carbon Monoxide and Hydrogen on the Ru(0001) Surface. *J. Phys. Chem. B* **2018,** *122*, 649-656.

37.	Riedl, W.; Menzel, D., Crowding and tilting in dense adsorbate layers; An ESDIAD investigation of CO on Ru(001) and Ni(110). *Surf. Sci.* **1985,** *163*, 39-50.

38.	McEwen, J.-S.; Eichler, A., Phase diagram and adsorption-desorption kinetics of CO on Ru(0001) from first principles. *J. Chem. Phys.* **2007,** *126*, 094701.

39.	Thomas, G. E.; Weinberg, W. H., High resolution electron energy loss spectroscopy of chemisorbed carbon monoxide and oxygen on the ruthenium (001) surface. *J. Chem. Phys.* **1979,** *70*, 954-961.

40.	Pfnür, H.; Menzel, D.; Hoffmann, F. M.; Ortega, A.; Bradshaw, A. M., High resolution vibrational spectroscopy of CO on Ru(001): The importance of lateral interactions. *Surf. Sci.* **1980,** *93*, 431-452.

41.	Williams, E. D.; Weinberg, W. H., The geometric structure of carbon monoxide chemisorbed on the ruthenium (001) surface at low temperatures. *Surf. Sci.* **1979,** *82*, 93-101.

25

42.   Pfnür, H.; Heier, H. J., Order-Disorder Phenomena in the System CO/Ru(001). *Ber. Bunsen-Ges. Phys. Chem* **1986,** *90*, 272-277.

43.   Zhao, P.; He, Y.; Cao, D.-B.; Wen, X.; Xiang, H.; Li, Y.-W.; Wang, J.; Jiao, H., High coverage adsorption and co-adsorption of CO and H 2 on Ru (0001) from DFT and thermodynamics. *Phys. Chem. Chem. Phys.* **2015,** *17*, 19446-19456.

44.   Trost, J.; Zambelli, T.; Wintterlin, J.; Ertl, G., Adsorbate-adsorbate interactions from statistical analysis of STM images: N/Ru(0001). *Phys. Rev. B* **1996,** *54*, 17850-17857.

45.   Zambelli, T.; Trost, J.; Wintterlin, J.; Ertl, G., Diffusion and Atomic Hopping of N Atoms on Ru(0001) Studied by Scanning Tunneling Microscopy. *Phys. Rev. Lett.* **1996,** *76*, 795-798.

46.   Lindroos, M.; Pfnür, H.; Held, G.; Menzel, D., Adsorbate induced reconstruction by strong chemisorption: Ru(001)p(2×2)-O. *Surf. Sci.* **1989,** *222*, 451-463.

47.   Stampfl, C.; Scheffler, M., Theoretical study of O adlayers on Ru(0001). *Phys. Rev. B* **1996,** *54*, 2868-2872.

48.   Renisch, S. Zur Diffusion adsorbierter Teilchen auf Einkristalloberflächen: Dynamische Untersuchungen mit dem Rastertunnelmikroskop. Freie Universität Berlin, Berlin, 1999.

49.   Ehrlich, G., Atomic Displacements in One- and Two-Dimensional Diffusion. *J. Chem. Phys.* **1966,** *44*, 1050-1055.

50.   Renisch, S.; Schuster, R.; Wintterlin, J.; Ertl, G., Dynamics of Adatom Motion under the Influence of Mutual Interactions: O/Ru(0001). *Phys. Rev. Lett.* **1999,** *82*, 3839-3842.

51.   Stampfl, C.; Scheffler, M., Energy barriers and chemical properties in the coadsorption of carbon monoxide and oxygen on Ru(0001). *Phys. Rev. B* **2002,** *65*, 155417.

52.   Deckert, A. A.; Brand, J. L.; Arena, M. V.; George, S. M., Surface diffusion of carbon monoxide on Ru(001) studied using laser-induced thermal desorption. *Surf. Sci.* **1989,** *208*, 441-462.

53.   van Santen, R. A.; Markvoort, A. J.; Filot, I. A. W.; Ghouri, M. M.; Hensen, E. J. M., Mechanism and microkinetics of the Fischer–Tropsch reaction. *Phys. Chem. Chem. Phys.* **2013,** *15*, 17038-17063.

54.   Böller, B.; Zeller, P.; Günther, S.; Wintterlin, J., High-Pressure CO Phases on Co(0001) and Their Possible Role in the Fischer–Tropsch Synthesis. *ACS Catal.* **2020,** *10*, 12156-12166.

26

1
2
3
4
5
6
7
8
9
10
11
12
13
14
15
16
17
18
19
20
21
22
23
24
25
26
27
28
29
30
31
32
33
34
35
36
37
38
39
40
41
42
43
44
45
46
47
48
49
50
51
52
53
54
55
56
57
58
59
60

Table of Contents Image

Diffusional traces of adsorbed oxygen atoms on a CO-covered Ru(0001) surface

27